SATCOM at Ka bands IN TROPOSPHERE:

Attenuation prediction and Complementary Cumulative Distribution Function for O3b mPower

Politecnico di Milano

Satellite Communication and Positioning Systems

Matteo Luciardello Lecardi

977701

March 2022

1.INTRODUCTION

The focus of the following report is devoted to implementing the MATLAB modelling for the evaluation of tropospheric propagation parameters, as predicted within Recommendation ITU-R P.618, for Earth-space systems operating in either direction, towards or from space.

The ITU recommendations' methods are applied to realistic scenarios of the most recent Earth stations and satellites' antennas, in order to evaluate how severely the atmospheric absorption is affecting these systems at operative carrier frequencies.

The main attenuation phenomena are analyzed so to get a proper estimation of the magnitude of propagation losses and how a certain value is likely to occur, presenting the time probability of exceedance over an average year or the worst month.

Particular attention is given to attenuation due to rain, clouds and tropospheric scintillation. The complementary cumulative distribution function (CCDF) is the time probability that the attenuation exceeds a given value, used to estimate the probability of outage for Telecommunications system link, design, or vice versa, if the availability is known, to find the maximum attenuation that the system shall withstand before outage.

Three ground stations have been chosen, located at tropical, medium and high latitudes, in order to obtain as much variety as possible, especially considering *rainfall rate* and *isotherm height*. Maps and digital data available in ITU-R P.837 and P.839 are the first approach to perceive the incidence of the geo locations diversity with respect to the rain occurrences (see annex 2 and 3).

2.O3b mPower MEO:Ka-band Link

Peculiarities

The O3b constellation interfaces with MEOLink Viasat Earth stations, specifically designed for O3b MEO, with its pair of 4.5m high-precision tracking Cassegrain reflectors, providing a high-performance Ka-band antenna system: operative carrier frequencies at downlink in the band from 17.8 to 19.3GHz and uplink from 27.6 to 29.1GHz, RHCP/LHCP (Right/Left Hand Circular Polarization) (O3b Networks Limited, Viasat Inc., 2017).

The station receivers are located respectively at 7.5°N 81°E (Sri Lanka) for low latitude analysis, 45°N -63°E (Canada) for medium latitude, 64.5°N -21°E (Iceland) for high latitude.

History

Originally announced in 2017, O3b mPower MEO communications system is a new constellation, consisting of 11 crafts: satellites № 1-3 launched on the 27th of February 2022 (Falcon 9 launcher, Space X), satellites 4-6 on target to launch in the second quarter of 2022, 7-9 in the second half of 2022 and 10-11 in 2024 (SES S.A., 2022).

This system will significantly increase the size, power and flexibility of the existing O3b (2013), serving nearly 96% of the total population, now operating between 50°N and 50°S latitudes.

The amendment Federal Communications Commission, Washington DC (2016) rules that the service coverage gets extended to all locations as far north as 70 degrees latitude. (Suzanne Malloy, 2016)

Application

O3b mPower MEO orbital height is 8000km, it is NGSO (Non-Geostationary) with latency as low as 150ms RTT (Round Trip Time), developed for mobile backhaul and cloud services, e.g Microsoft Azure is one of the most prominent upcoming services available through the O3b universe. Estimated availability is 99.5%., throughout per service of 50Mbps to 1Gbps (SES S.A., 2020)

3.The propagation phenomena

The propagation phenomena concerning Earth-space links mainly originate in the ionosphere and in the troposphere. The effects taking place in the former can influence systems operating below 3GHz, the latter above 3 GHz, critically affecting their performance.

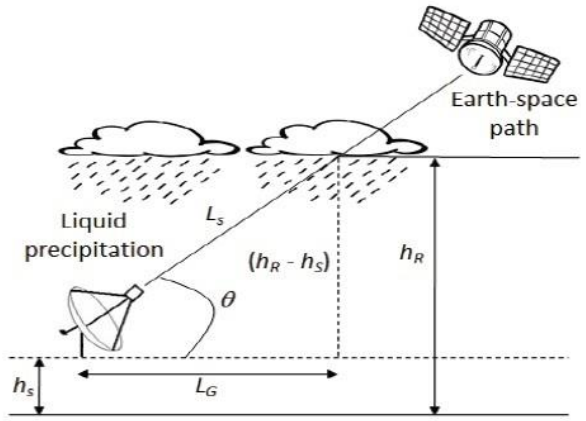

Figure 1. Schematic diagram of the Earth-Space path

Troposphere starts at the Earth's surface and extends up to c.a. 30km. (NASA, Holly Zell, 2013) Being the most dense part of the atmosphere, almost all weather phenomena occur in this region.

The aforementioned propagation loss is a sum of different contributions, each of them presenting different characteristics as a function of frequency, geographic location and elevation angle.

Attenuation due to precipitation

Hydrometeor *absorption* is the dominant phenomenon causing power loss within the spectrum between 10GHz and 30GHz, although when propagating trough rain, snow and ice droplets, radiowaves suffer from power loss due to *hydrometeor scattering,* and combined effect of absorption and scattering results in power losses proportional in dB to the square of frequency. (Athanasios D. Panagopoulos, January 2004)

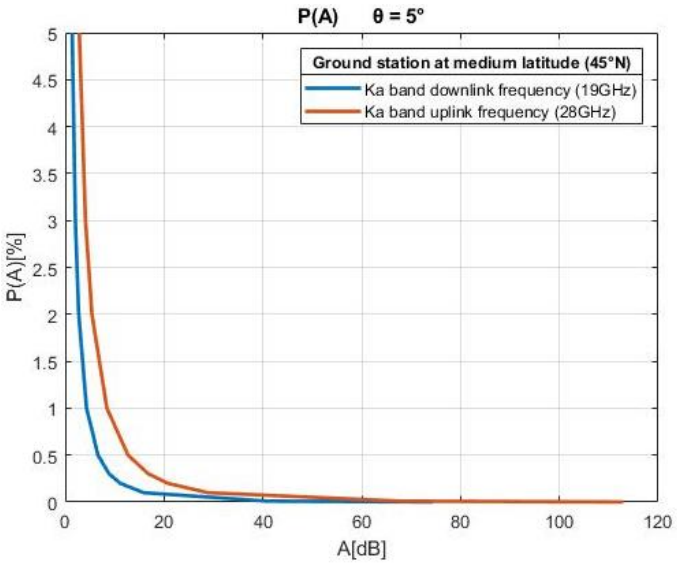

Figure 2. CCDF percentage of total time for satellite link operating in New Scotland, Canada (elevation angle = 5°, RHCP/LHCP) The curve of P(A) at uplink frequency (28GHz) has been predicted from long-term frequency scaling (MATLAB [3])

Elevation and polarization angles are mainly responsible for the depth of rain fades, as well as rainfall rate and droplets size distribution affect the rain attenuation, especially at tropical locations.

In Fig. 2 the ITU-R model predicts the annual exceedance probability of rain attenuation for both downlink and uplink frequencies, for the link operating at mid latitude, in the lowest elevation angle reasonably admissible.

A_p, function of the cumulative distribution of probability from 0.001% to 5%, provides an estimate of long-term statistics for rain attenuation and it is calculated as cited in Annex 1, where A_{001} is the predicted attenuation exceeded for 0.01 of an average year.

The logarithmic scale is rather preferrable for the time probability of exceedance to better help distinguishing the behaviour of the curves, and it is presented later on.

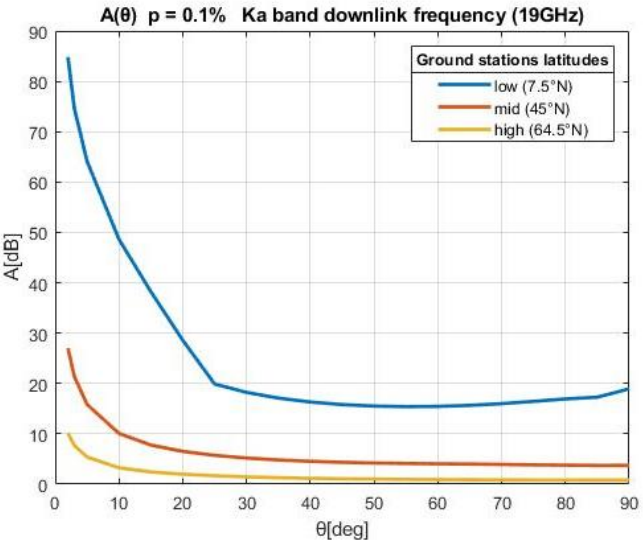

Figure 3. Attenuation due to rain at 3 locations vs elevation angle, fixed time probability of exceedance at 0.1%, frequency for O3b downlink within the Ka band (MATLAB [1])

In Fig. 3 the rain attenuation over elevation angle shows that the losses are mostly minimized during zenith link, on the other hand, the lower the elevation angle, the more the systems are affected by attenuation.

It is also noticeable that approaching the right half of the graph, the attenuation value is nearly constant.

Consequently, it's rather helpful to visualize the lowest elevation angle as the worst occurrence along the spacecraft's orbital path, so to cope with the worst case link budget design.

Following the ITU-R 618 Recommendation, the probability of non-zero rain attenuation on a given slant path $P(A > 0)$ is function of the *complementary bivariate normal distribution* c_B, and the annual probability of rain at the earth station location $P_{0_{annual}}$:

$$c_B = \frac{1}{2\pi\sqrt{1-\rho^2}} \int_{\alpha}^{\infty} \int_{\alpha}^{\infty} e^{-\frac{x^2-2\rho xy+y^2}{2(1-\rho^2)}} dxdy$$

where α is the *normal inverse cumulative distribution function* of $P_{0_{annual}}/100$, which is easily computed via MATLAB as

$$\alpha = Q^{-1}(p) = \sqrt{2}\,\mathrm{erfcinv}(2p)$$

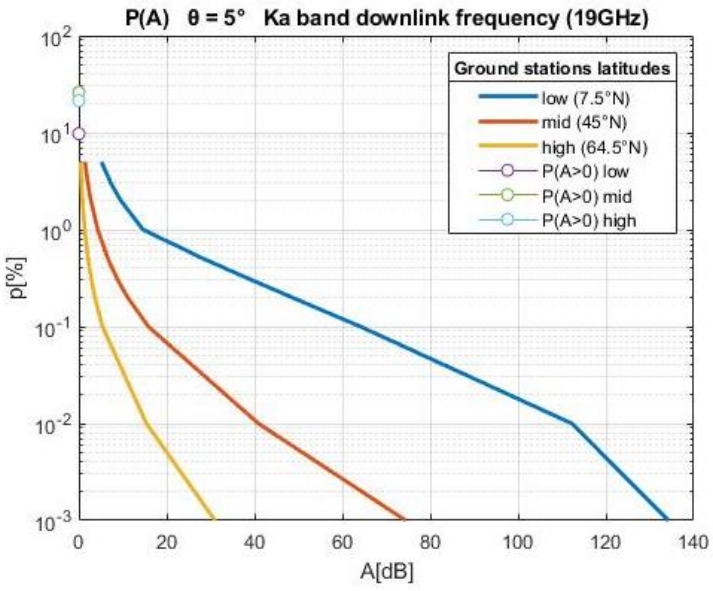

Figure 4. Percentage of total time vs Rain attenuation for 3 different locations, and probability of non-zero attenuation on a slant path P(A>0) values (MATLAB [2]) (see annex 4 for the curves at different elevation angles)

Following *Drezner* and *Wesolowsky* method, the c_B integral is computed though Gaussian quadrature based on K points, requiring calculation of K values of exponents. Cases for K = 2 and K = 3 have been evaluated and the results differ for an error in the order of 10^{-3}. (Zvi Drezner, 1990)

In Figure 4 the semi logarithmic plot shows that on average at tropical latitudes the higher rainfall rate causes the attenuation levels to exceed much higher values than in the other locations.

Seasonal variations – worst month

A relevant system design requirement is the attenuation value exceeded for the *average annual worst-month time percentage* p_w, which has upper and lower boundaries, depending on the geographical location of the receiver.

Figure 5 shows that in the same condition (carrier frequency and elevation angle, polarization), attenuation exceeding p_w is much lower than the attenuation over the average annual time.

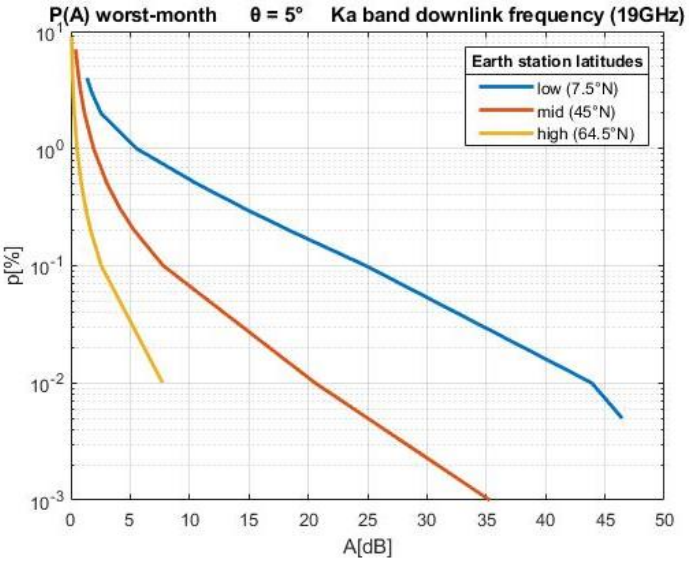

Figure 5. Average annual worst-month time percentage vs Attenuation, in 3 different locations, at the worst elevation angle (MATLAB [4])

Site Diversity Protection scheme

Diversity protection schemes are countermeasures to mitigate rain fades. They are able to re-route traffic to alternate Earth stations, or to access to a different satellite, so to improve the system reliability, because the largest attenuation values are caused by intense rain cells extending horizontally only for a few kilometers. The system link O3b mPower and Viasat MEOLink is balanced as long as the attenuation thresholds are equal on the two

links., therefore the site diversity performance can be predicted from a simplified model valid for separation distances up to 20km, as follows.

The *Diversity gain* represents the increase in SNR (Signal to Noise Ratio) obtained with the application of a Site Diversity scheme.

In Annex 5 this parameter is shown as function of separation distance between the two sites, frequency, elevation angle and azimuth, over the attenuation. The *net diversity gain* has been designed considering fixing certain values for each case, so to understand the behaviour of the function with respect to each variable: d = 15km, f = 28GHz, θ = 45°, ψ = 45°.

Attenuation due to Scintillation

This effect causes variations in magnitude and profile of the refractive index of the troposphere, which depend on the water vapour content of the atmosphere. The fluctuations increase with frequency and path length, and decrease with antenna beamwidth.

Three methods have been employed to predict the fading due to amplitude scintillation for different parts:

1) amplitude scintillation fading at free-space elevation angle $\theta \geq 5°$ (Fig.6 & Annex 6, 7, 8);
2) amplitude fading for fades $A \geq 25dB$ and $\theta < 5°$ (Annex 9);
3) amplitude in transition region $A < 25dB$ and $\theta < 5°$ (Annex 10).

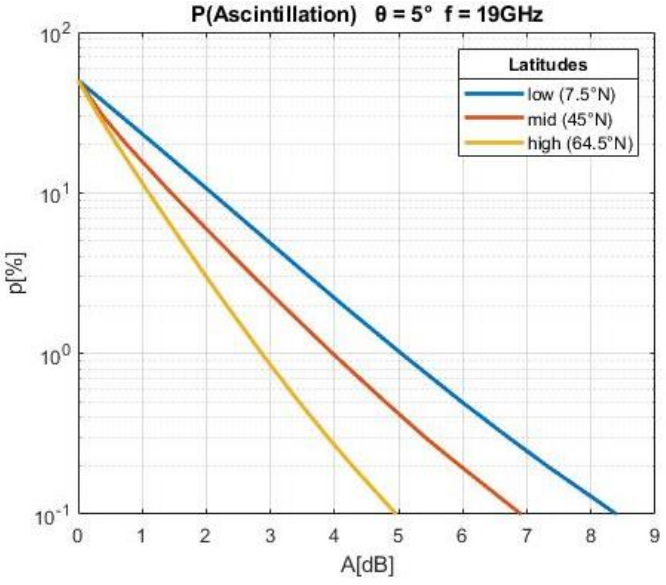

Figure 6. Average annual time percentage of exceedance vs scintillation fade for 3 sites at the worst reasonable elevation angle ϑ = 5° (MATLAB[7])

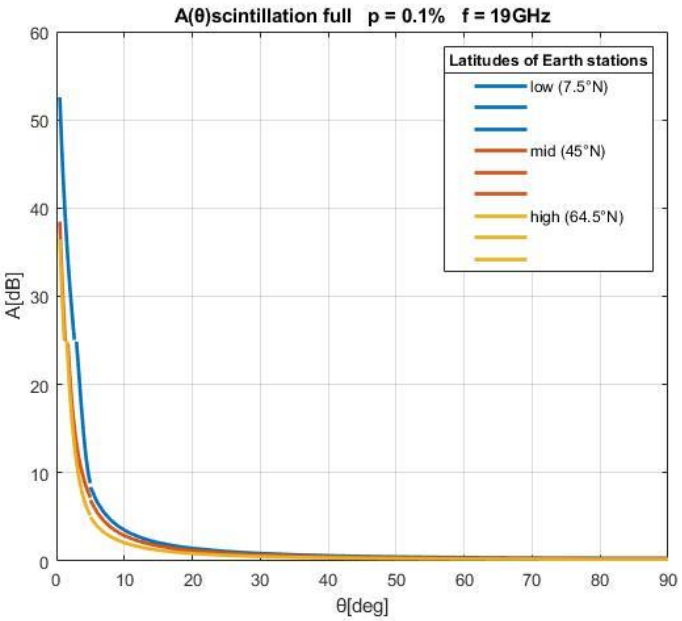

Figure 7. Scintillation fading vs elevation angle for 3 sites, showing together the models for the 3 regions, so to cover the full phenomenon for 0° < ϑ < 90° (MATLAB[12])

In order to compare the scintillation fading with attenuation due to rain, Fig.6 shows the analogue scenario of Fig 4: the curves are computed with the first methodology, in the range above 5 degrees of elevation angle till 90 degrees. It's clear how this phenomenon has a lighter impact on the systems than attenuation due to rainfall.

The Annexes 7 and 8 present few more cases at higher elevation angles, confirming that the probability of exceedance decreases the higher the elevation.

To be exhaustive, the result of the three computations has been linearly plotted altogether in Fig.7, so to offer a direct comparison to rain attenuation A(θ) shown in Figure 3, at the same geographical sites, probability of exceedance, and carrier frequency. Therefore, at very low elevation angles, still the fading impairment is less relevant than the rain one. In Annex 11 the same elements have been scale on a semilogarithmic plot.

Attenuation due to Clouds and fog

The liquid water content of clouds is the physical cause of clouds attenuation

ITU-R P.840 prediction models and local data shall be selected to estimate cloud attenuation along slant paths for Earth-Space link, used to generate the curves in Fig. 8

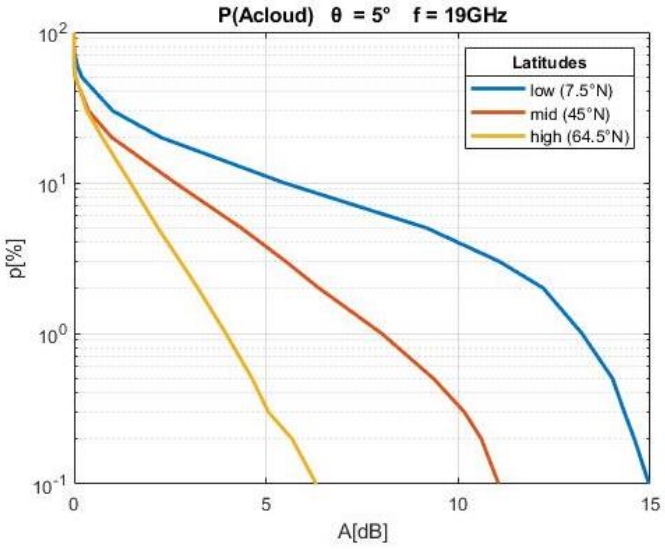

Figure 8. Time probability of exceedance vs attenuation due to clouds and fog for a satellite link operating at different latitudes (MATLAB[13]) (Annex 12 shows the same curves at different elevation angles, annex 13 shows different frequencies)

4.Total attenuation

Multiple sources of atmospheric attenuation occurring simultaneously.

The probability of exceedance for each phenomenon is directly compared to each other in Figure 9, before the computation of their sum, in Figure 10, calculated as follows:

$$A_T(p) = \sqrt{[A_R(p) + A_C(p)]^2 + A_S^2(p)}$$

where:

$$Ac(p) = Ac(1\%) \qquad \text{for } p < 1.0\%$$

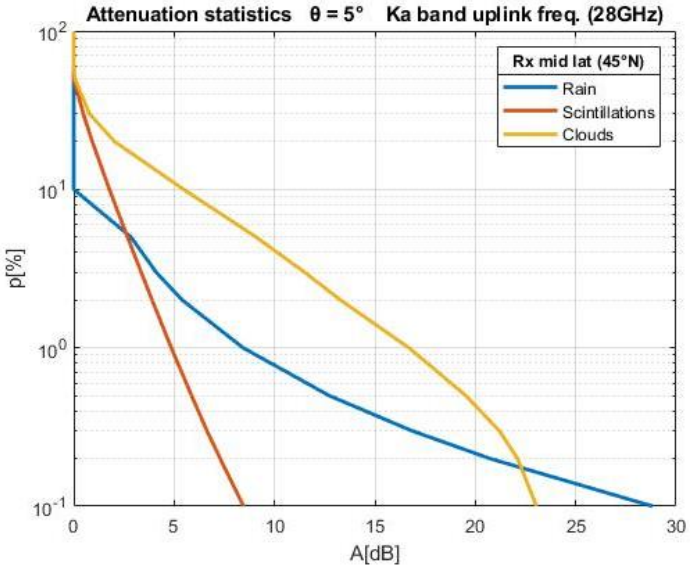

Figure 9. Prediction of tropospheric attenuation, for circular polarization, rain attenuation and non-rainy components (MATLAB[16])

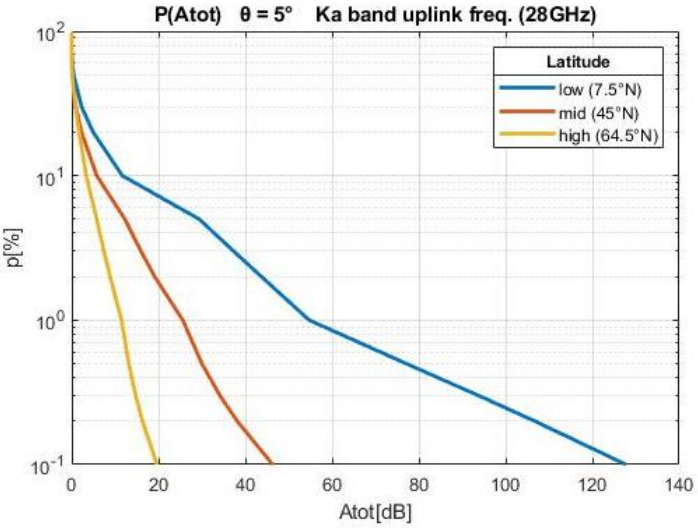

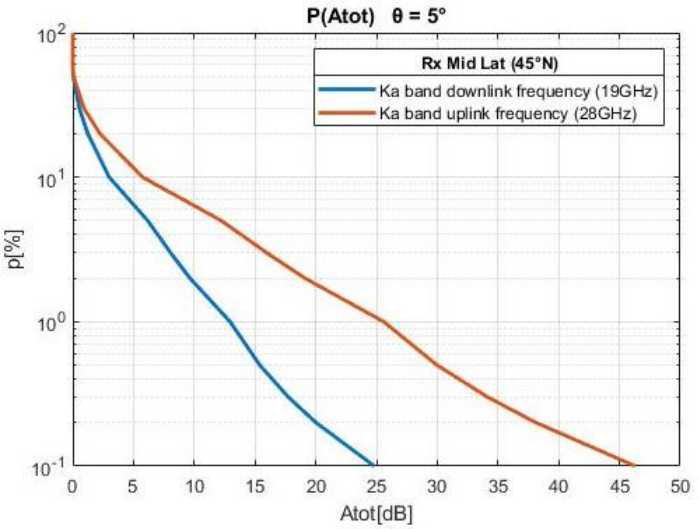

Figure 10. Statistical combination of all tropospheric contributions (state-of-the-art) (MATLAB[15])

5.Noise Temperature

Emission noise increases along with attenuation, and for earth stations this may have a greater impact on the SNR (Signal to Noise) ratio. The CCDF of the *sky noise temperature* T_{sky} at ground station antenna is represented in Fig. 11.

$$T_{sky} = T_{mr}\,(1 - 10^{-A/10}) + 2.7 \times 10^{-A/10} \quad \text{K}$$

where A is the total attenuation aforementioned, scintillation fading excluded, and T_{mr} is the atmospheric mean radiating temperature i.e., 275K in absence of local data.

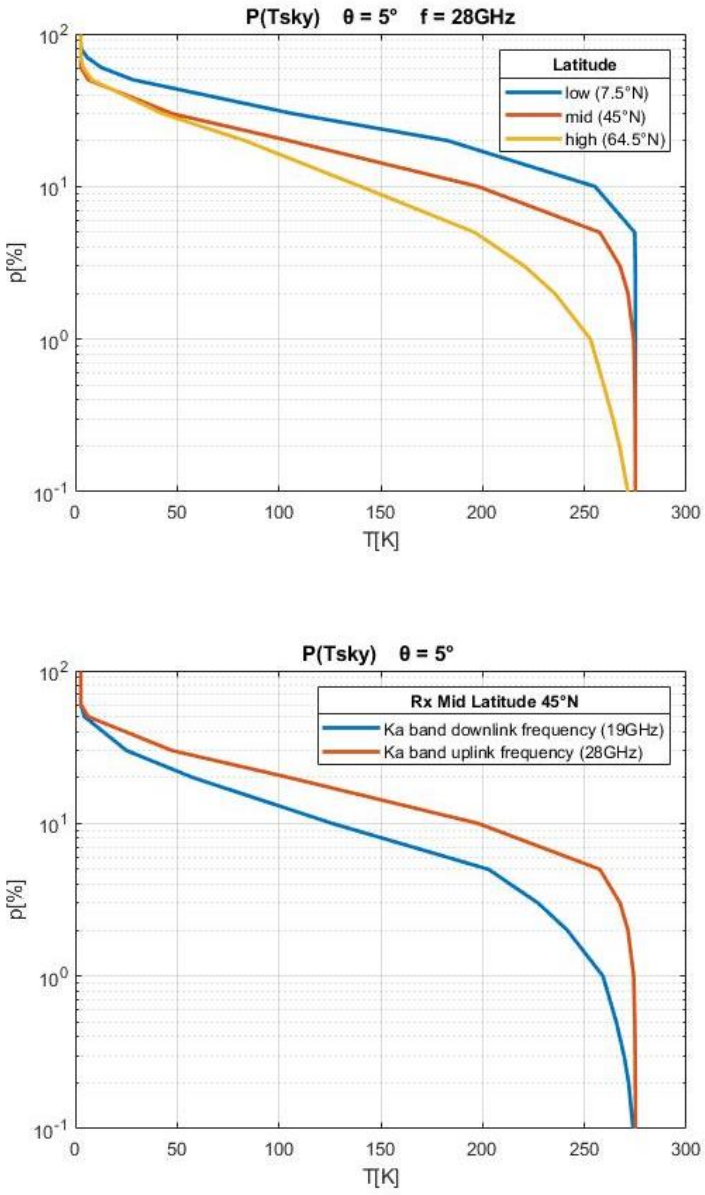

Figure 11. Probability of exceedance of the sky noise temperature at different latitudes and carrier frequencies, in the worst elevation angle condition ϑ = 5° (MATLAB[17])

6.System Design

O3b mPower constellation declares as "SLA commitment" (Service-Level Agreement) that the link will ensure an availability of 99.5%.

This means that the link outage probability at 0.5% will cause c.a. 1d 19h 48min of disconnection over a period of one year, due to tropospheric propagation effects affecting the link.

Considering the total attenuation estimations shown in the previous paragraphs, this probability is exceeded by different values of attenuation, depending on elevation angle, location and whether it is an uplink or a downlink carrier frequency to be considered.

At elevation angle of θ = 5°, the attenuation exceeding p = 0.5% for the different stations is:

A tot [dB]	Low Lat	Mid Lat	High Lat
DwnLink 19GHz	42.0648	15.3954	6.9618
UpLink 28GHz	77.0708	29.9811	13.1234

Table 1. Total Attenuation exceeded for 0.5% of time at ϑ = 5° at different ground stations (MATLAB[A05])

Therefore, the system shall mitigate the attenuation of at least 77.0708 dB to satisfy the user requirement of 99.5% availability for the worst location and elevation angle available.

From the total attenuation, the Noise Temperature exceeded 0.5% of the total time is calculated and reported in Table 2.

Tsky [K]	Low Lat	Mid Lat	High Lat
DwnLink 19GHz	274.9813	265.6253	207.3886
UpLink 28GHz	275	274.685	259.4297

Table 2. Sky noise temperature exceeded for 0.5% of the time at ϑ = 5° at different ground stations (MATLAB[T05])

ANNEX

$$A_p = A_{0.01}\left(\frac{p}{0.01}\right)^{-(0.655 + 0.033\ln(p) - 0.045\ln(A_{0.01}) - \beta(1-p)\sin\theta`} \quad \text{dB}$$

Annex 1. Estimated attenuation to be exceeded for other percentages of an average year, from 0.001% to 5%

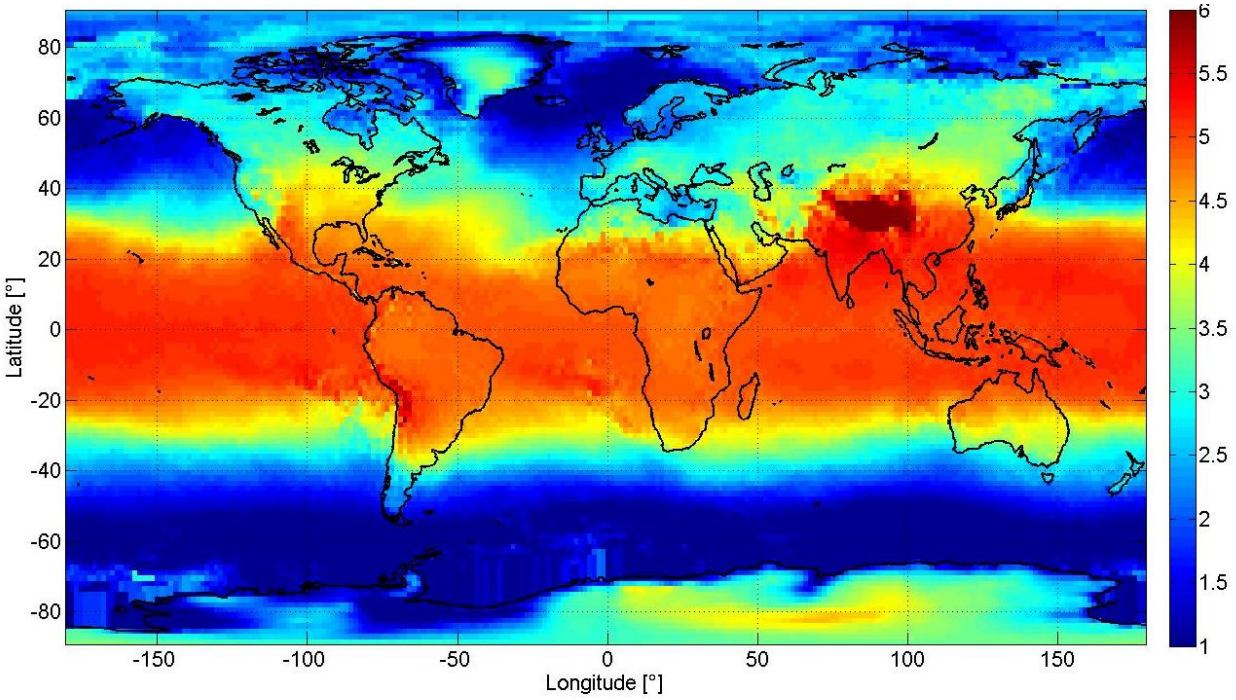

Annex 2. ITU-R P.839 mean annual 273.15K isotherm height above mean see level map

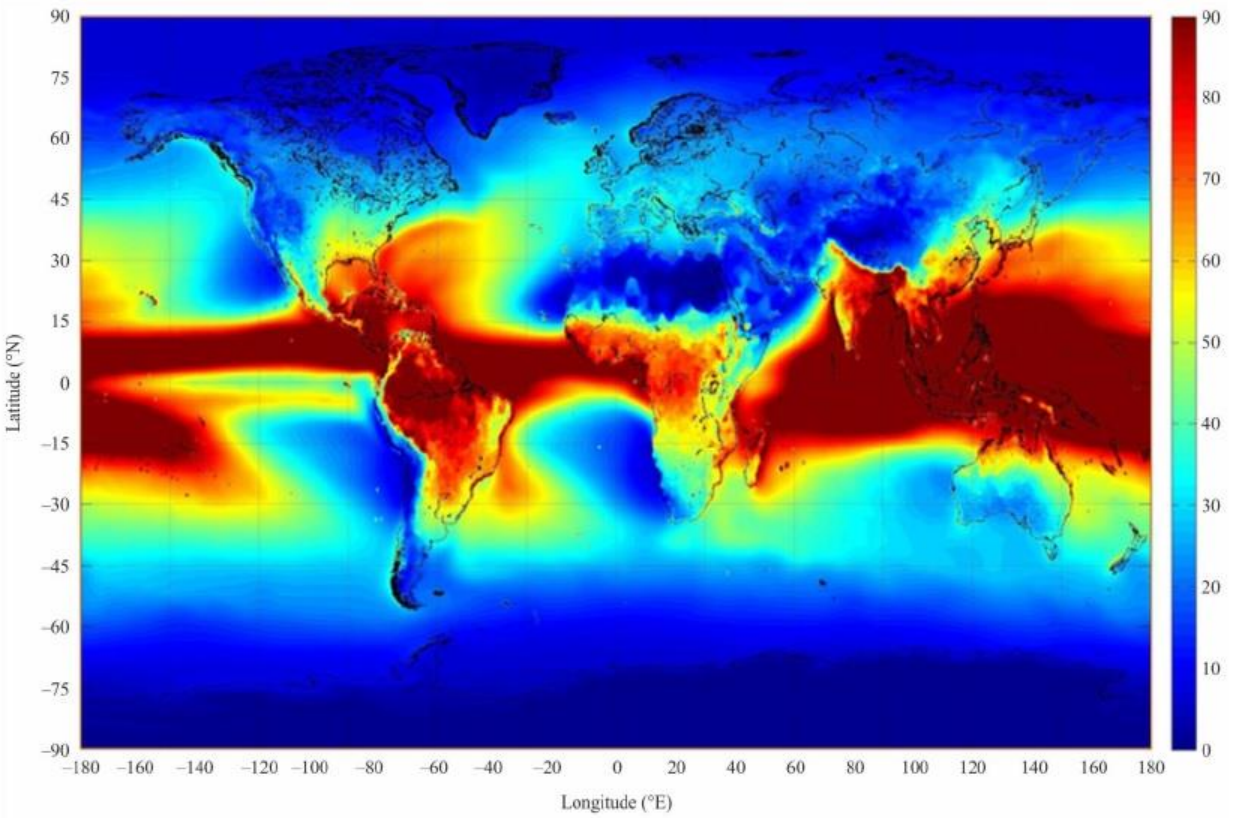

Annex 3. ITU-R P.837 rainfall rate exceeded for 0.01% of an average year

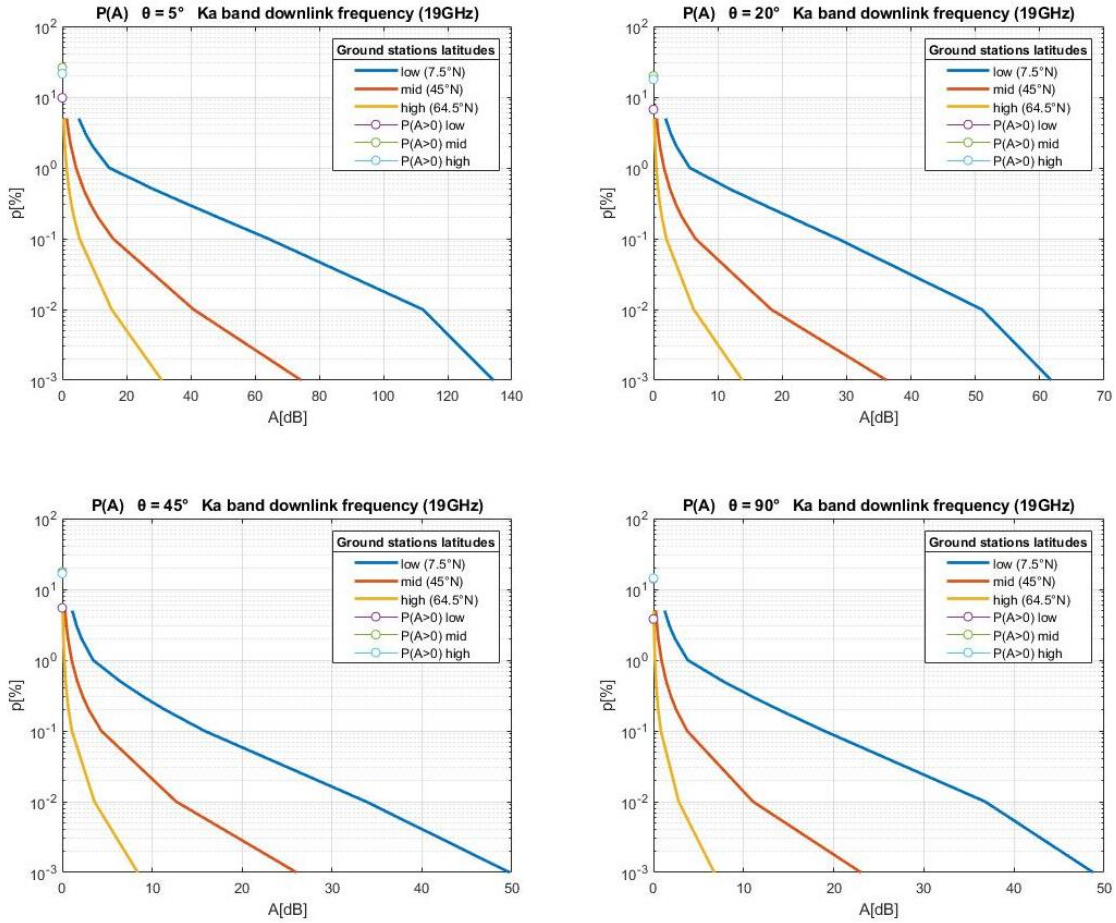

Annex 4. Annual probability of exceedance vs Attenuation . Notice that changing the elevation angle from 45° to 90°, the attenuation doesn't drop significantly, as expected from Figure 3 analysis (MATLAB[2])

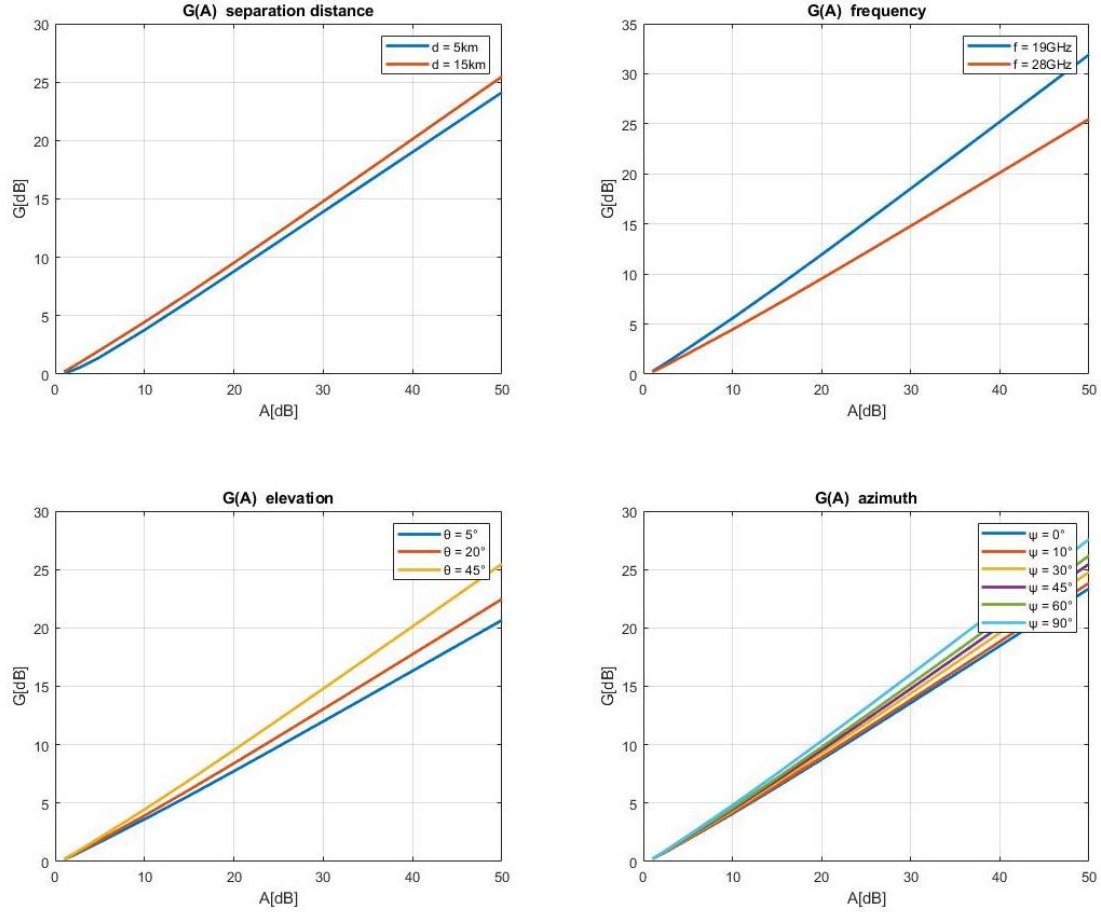

Annex 5. Net Diversity gain vs Rain attenuation (MATLAB[5])

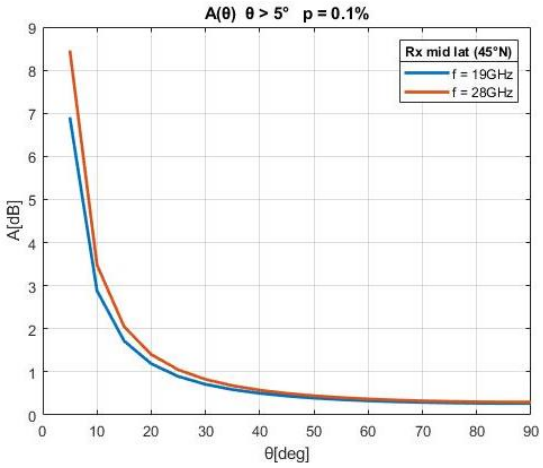

Annex 6. Scintillation fading vs elevation angle, in the region ϑ ≥ 5. The difference in attenuation between the downlink and uplink frequencies are appreciable only in the left half of the curves (MATLAB[6])

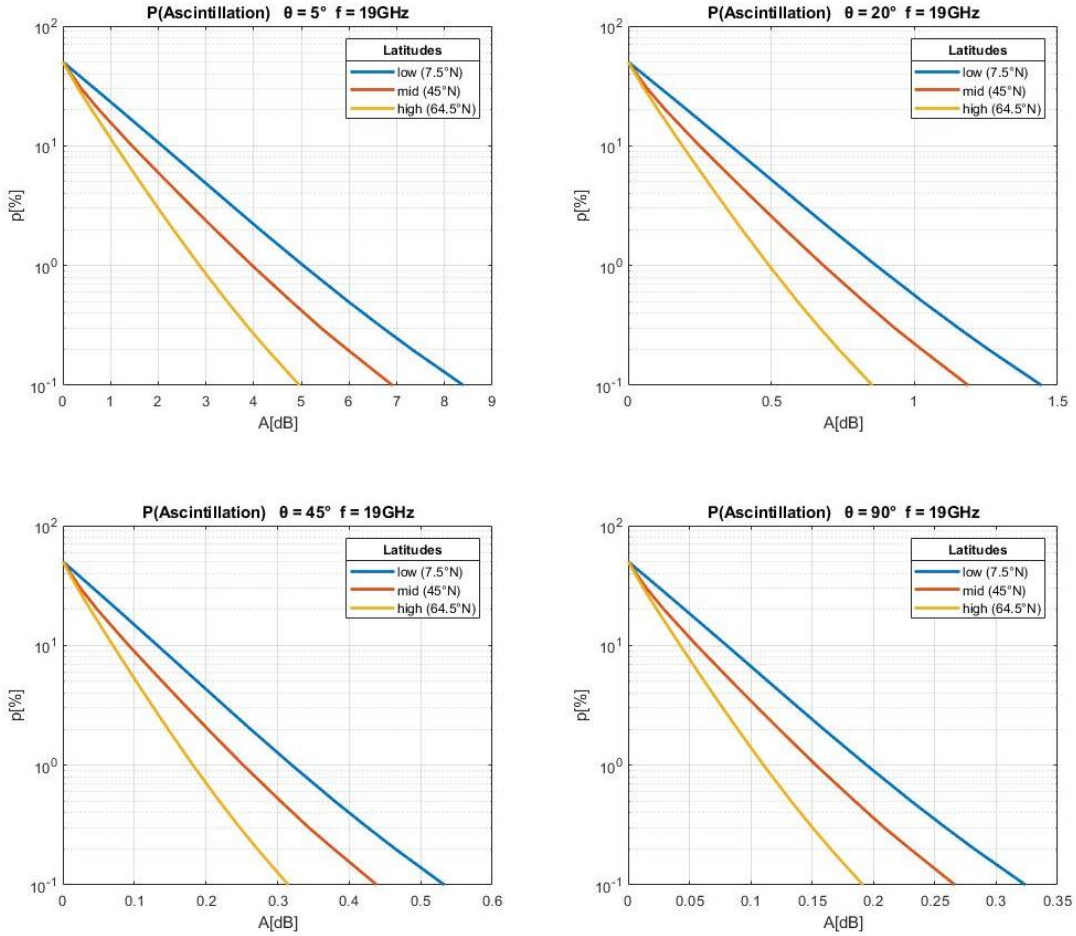

Annex 7. Average annual time percentage of exceedance vs scintillation fading at 3 geographical sites, at downlink carrier frequency, as expected from Annex 5, the attenuation is not very much affected by elevation angle from ϑ = 45° to zenith (MATLAB[7])

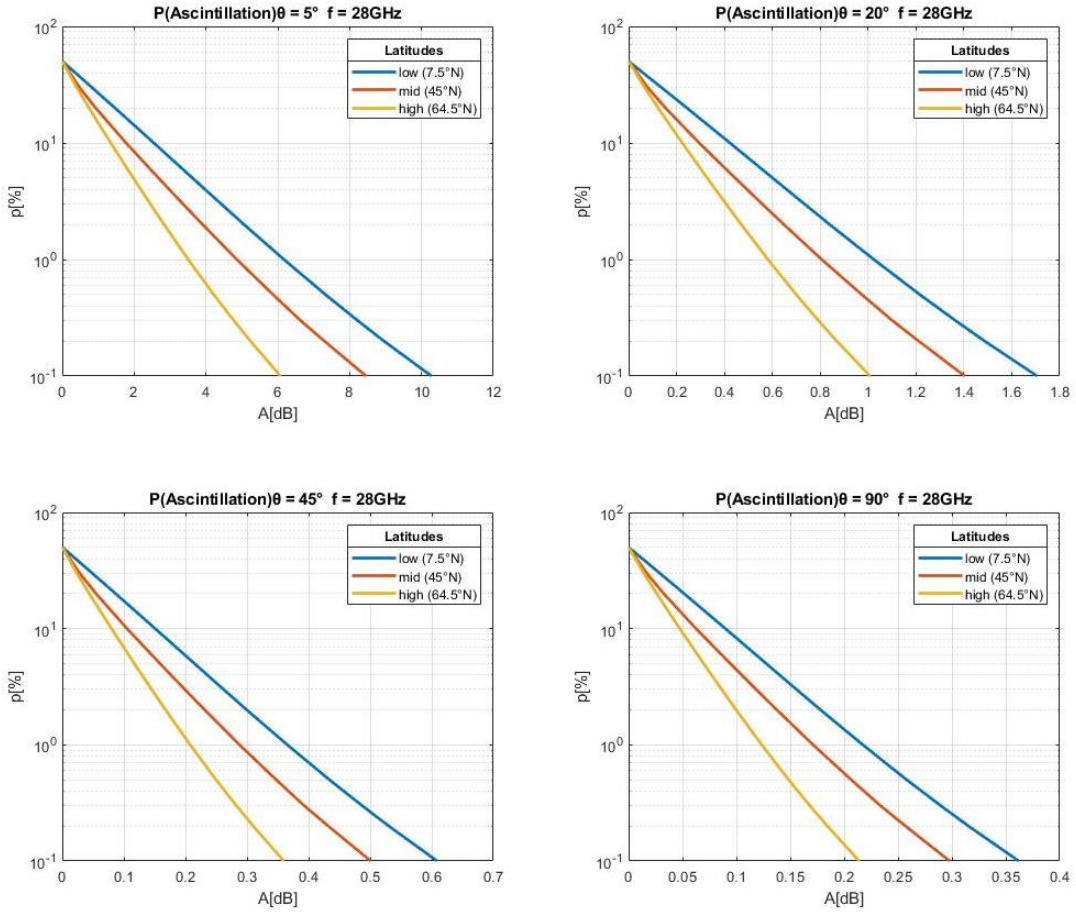

Annex 8. Average annual time percentage of exceedance vs scintillation fading at 3 geographical sites, at uplink carrier frequency (MATLAB[8])

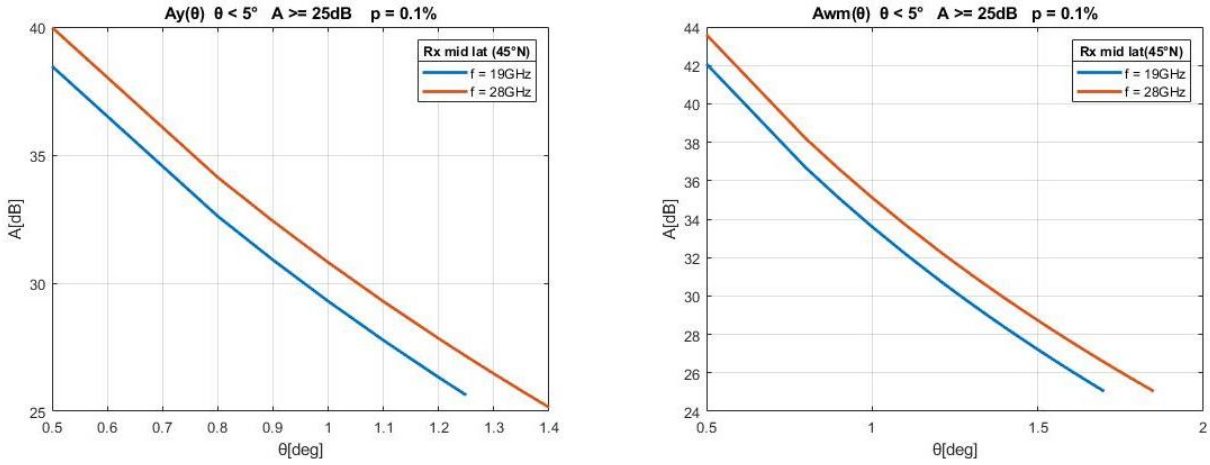

Annex 9. Scintillation fading vs elevation angle, in the region $\vartheta < 5°$ $A \geq 25dB$, for average year and worst month (MATLAB[9])

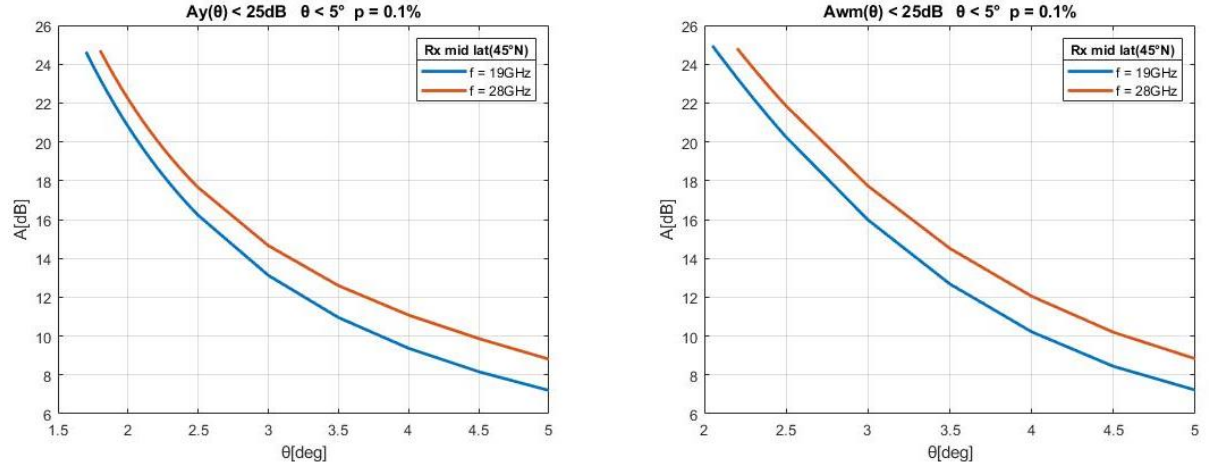

Annex 10. Scintillation fading vs elevation angle, in the region $\vartheta < 5°$ $A < 25dB$ (MATLAB[10])

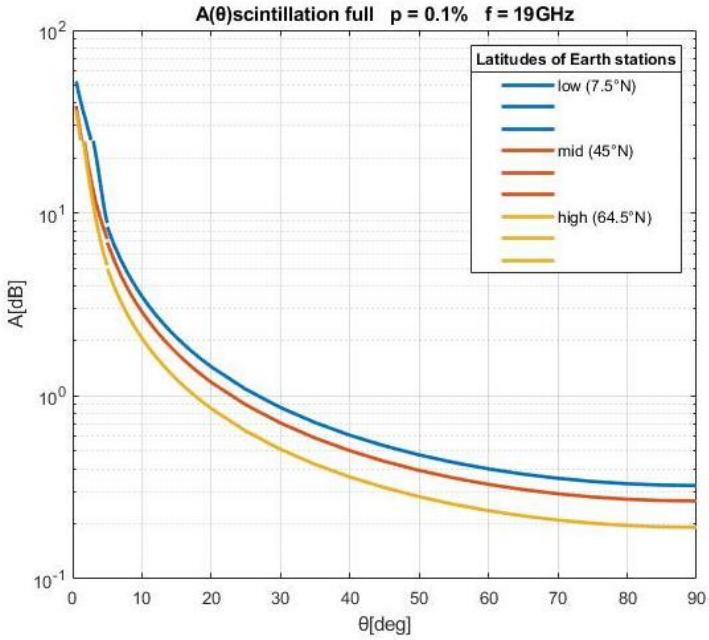

Annex 11. Scintillation fading vs elevation angle for 3 sites, showing together the models for the 3 regions, so to cover the full phenomenon for 0° < ϑ < 90°, semilogarithmic scale for better distinction of the segments (MATLAB[12Bis])

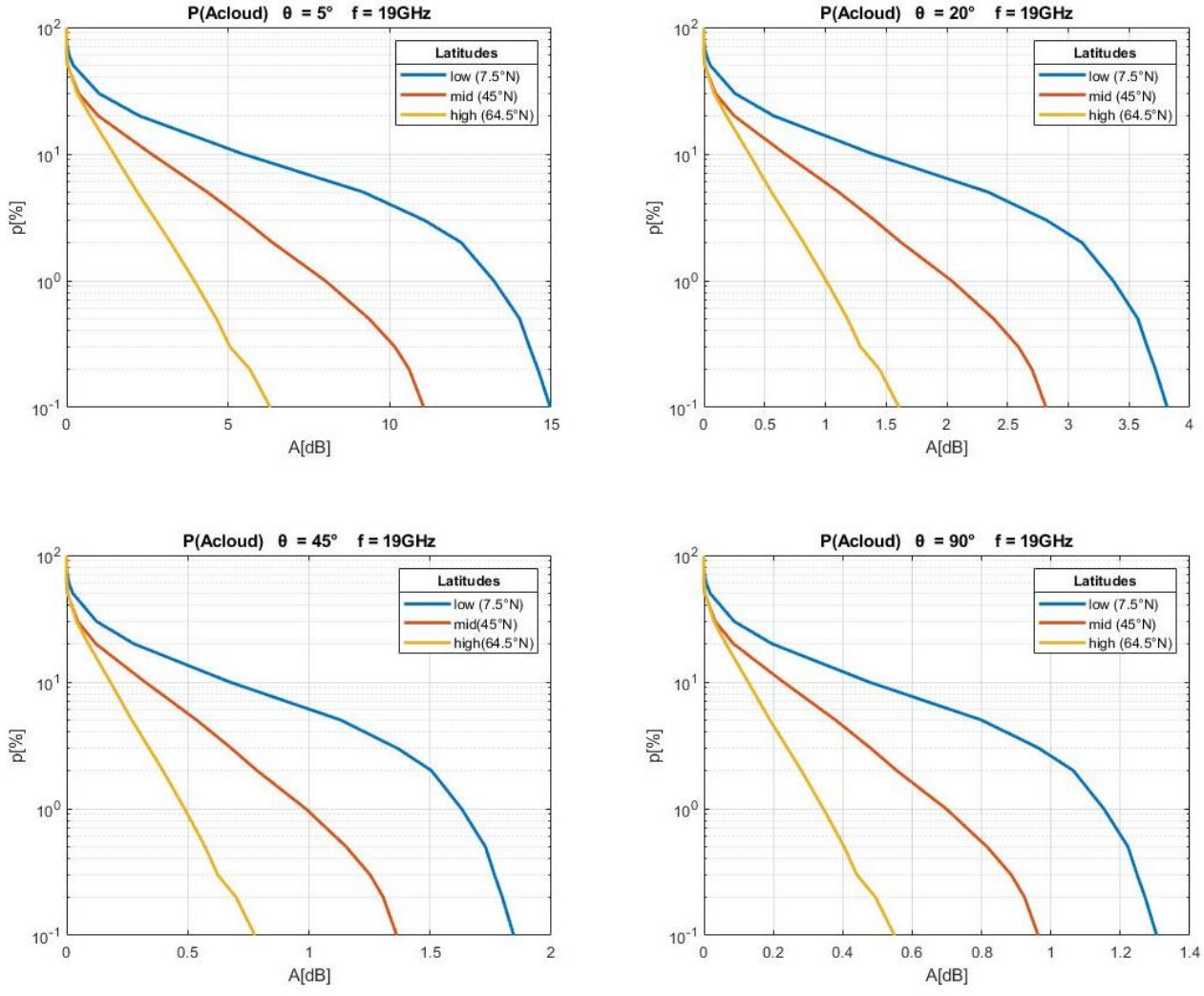

Annex 12. Time probability of exceedance vs attenuation due to clouds and fog (MATLAB[13])

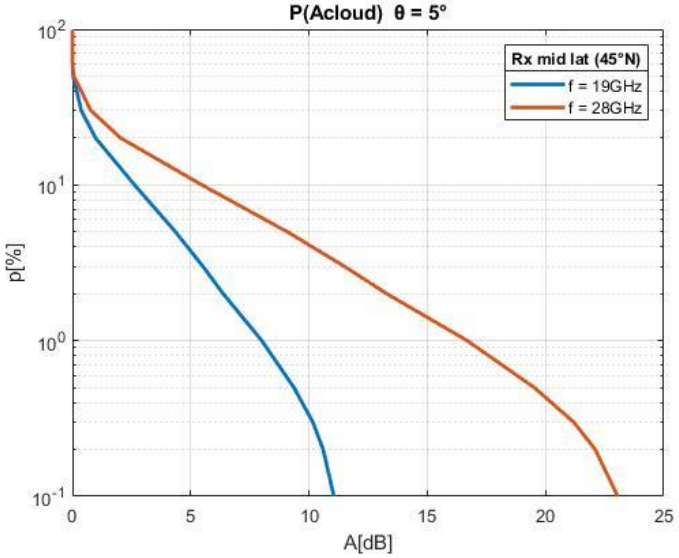

Annex 13. Time probability of exceedance vs attenuation due to clouds and fog at La band downlink and uplink frequencies (MATLAB[14])

REFERENCES

Athanasios D. Panagopoulos, P.-D. A. (January 2004). Satellite communications at KU,KA and V bands: Propagation impairments and mitigation techniques. *IEEE Communications Surveys & Tutorials*.

International Telecommunication Union. (2005). *Recommendation ITU-R P. 838. Specific attenuation model for rain for use in prediction mehtods.* Retrieved from itu.int: https://www.itu.int/rec/R-REC-P.838-3-200503-I/en

International Telecommunication Union. (2013, 9). *Recommendation ITU-R P.839-4. Rain height model for prediction methods.* Retrieved from itu.int: https://www.itu.int/rec/R-REC-P.839-4-201309-I/en

International Telecommunication Union. (2015, 7). *Recommendation ITU-R P678-3 Characterization of the variability of propagation phenomena and estimation of the risk associated with propagation margin.* Retrieved from itu.int: https://www.itu.int/rec/R-REC-P.678-3-201507-I/en

International Telecommunication Union. (2017, 12). *Recommendation ITU-R O.618-13 Propagation data and prediction methods required for the design of Earth-space telecommunication systems.* Retrieved from itu.int: https://www.itu.int/rec/R-REC-P.618-13-201712-I/en

International Telecommunication Union. (2017, 12). *Recommendation ITU-R P.834-9. Effects of tropospheric refraction on radiowave propagation.* Retrieved from itu.int: https://www.itu.int/rec/R-REC-P.834-9-201712-I/en

International Telecommunication Union. (2017, 6). *Recommendation ITU-R P.837-7. Characteristics of precipitatiom for propagation modelling.* Retrieved from itu.int: https://www.itu.int/rec/R-REC-P.837-7-201706-I/en

International Telecommunication Union. (2019, 8). *Recommendation ITU-R P.1057-6. Probability distributions relevant to radiowave propagation modelling.* Retrieved from itu.int: https://www.itu.int/rec/R-REC-P.1057-6-201908-I/en

International Telecommunication Union. (2019, 8). *Recommendation ITU-R P.453-14. The radio refractive index: its formula and refractivity data.* Retrieved from itu.int: https://www.itu.int/rec/R-REC-P.453/en

International Telecommunication Union. (2019, 8). *Recommendation ITU-R P.840-8. Attenuation due to clouds and fog.* Retrieved from itu.int: https://www.itu.int/rec/R-REC-P.840-8-201908-I/en

International Telecommunication Union. (2019, 08). *Recommendation ITU-R P.841-6. Conversion of annual statistics to worst-month statistics.* Retrieved from itu.int: https://www.itu.int/rec/R-REC-P.841-6-201908-I/en

International Telecommunication Union. (2021, 9). *Recommendation ITU-R P.1144-11. Guide to the application of the propagation methods of Radiocommunication Study Group 3.* Retrieved from itu.int: https://www.itu.int/rec/R-REC-P.1144-11-202109-I/en

Krebs, G. (2022, February 14). *D. "O3b mPower 1, ..., 11 (O3b 21, ..., 31)". Gunter's Space Page*. Retrieved from Gunter's Space Page: https://space.skyrocket.de/doc_sdat/o3b-21.htm

NASA, Holly Zell. (2013, January 22). *Earth's Atmospheric Layers.* Retrieved from nasa.gov: https://www.nasa.gov/mission_pages/sunearth/science/atmosphere-layers2.html

O3b Networks Limited, Viasat Inc. (2017). *MEOLink.* Retrieved from viasat.com:

https://www.viasat.com/content/dam/us-site/antenna-systems/documents/meolink_antenna_datasheet_007_web.pdf

SES S.A. (2020, December). *Insight Paper-Redifining network services with O3b mPower.* Retrieved from ses.com: http://go.ses.com/rs/766-HRP-002/images/Insight%20paper%20-%20O3b%20mPOWER.pdf?mkt_tok=NzY2LUhSUC0wMDIAAAGC9fxnLg5r_Piwb2C74SGwiPzDGhKHRHgOccDNpmuilBfb4cXAtiD_w0fjyeWt3s0Rzu-4RM5YgnZsBZh5jjZZYH3lhrDZxKOjZ9h2rVM

SES S.A. (2020, August). *O3b mPOwer-Press Factsheet.* Retrieved from ses.com: https://www.ses.com/sites/default/files/2020-08/SES_O3b%20mPOWER_Newsroom_Factsheet.pdf

SES S.A. (2022, February 27). *Launches.* Retrieved from ses.com: https://www.ses.com/our-coverage/launches

SES S.A. (2022, February 24). *Press Release SES Full Year 2021 Results.* Retrieved from SES.com: https://www.ses.com/sites/default/files/2022-02/SES%20Full%20Year%202021%20Results_0.pdf

Suzanne Malloy, K. H. (2016, November 15). *US Ka-band NGSO Processing Round - Amendment - Legal O3b Narrative.* Retrieved from http://personal.ee.surrey.ac.uk/Personal/L.Wood/O3b-polar/o3b-narrative.pdf

Zvi Drezner, G. O. (1990). On the computation of the bivariate normal integral. *Journal of Statistical Computation and Simulation*, 35:1-2, 101-107.

CONTENTS